A&A 442, 29–41 (2005)
DOI: 10.1051/0004-6361:20053232

Astronomy & Astrophysics

Internal dynamics of the $z \sim 0.8$ cluster RX J0152.7−1357⋆

M. Girardi[1], R. Demarco[2,3], P. Rosati[2], and S. Borgani[1]

[1] Dipartimento di Astronomia, Università degli Studi di Trieste, via Tiepolo 11, 34100 Trieste, Italy
e-mail: girardi@ts.astro.it
[2] ESO-European Observatory, Karl-Schwarzschild-Str. 2, 85748 Garching, Germany
[3] Department of Physics & Astronomy, Johns Hopkins University, 3400 N. Charles Street, Baltimore, MD 21218, USA

Received 12 April 2005 / Accepted 1 June 2005

ABSTRACT

We present the results from the dynamical analysis of the cluster of galaxies RX J0152.7−1357, which shows a complex structure in its X-ray emission, with two major clumps in the central region and a third clump in the Eastern region. Our analysis is based on redshift data for 187 galaxies. We find that RX J0152.7−1357 appears as a well isolated peak in the redshift space at $z = 0.836$, which includes 95 galaxies recognized as cluster members. We compute the line-of-sight velocity dispersion of galaxies, $\sigma_V = 1322^{+74}_{-68}$ km s^{-1}, which is significantly larger than what is expected in the case of a relaxed cluster with an observed X-ray temperature of 5-6 keV. We find evidence that this cluster is far from dynamical equilibrium, as shown by the non Gaussianity of the velocity distribution, the presence of a velocity gradient and a significant substructure. Our analysis shows that the high value of σ_V is due to the complex structure of RX J0152.7−1357, i.e. to the presence of three galaxy clumps of different mean velocities. Using optical data we detect a low-velocity clump (with $\sigma_V = 300$–500 km s^{-1}) in the central southwest region and a high-velocity clump (with $\sigma_V \sim 700$ km s^{-1}) in the Eastern region, corresponding well to the South–West and East peaks detected in the X-ray emission. The central North–East X-ray peak is associated to the main galaxy structure with a velocity which is intermediate between those of the other two clumps and $\sigma_V \sim 900$ km s^{-1}. The mass of the whole system within 2 Mpc is estimated to lie in the range $(1.2$–$2.2) \times 10^{15}\ M_\odot$, depending on the model adopted to describe the cluster dynamics. Such values are comparable to those of very massive clusters at lower redshifts. Analytic calculations based on the two-body model indicate that the system is most likely bound and currently undergoing merging. In particular, we suggest that the southwestern clump is not a small group, but rather the dense cluster-core of a massive cluster, most likely destined to survive tidal disruption during the merger.

Key words. galaxies: clusters: general – galaxies: clusters: individual: RX J0152.7−1357 – galaxies: distances and redshifts – cosmology: observations

1. Introduction

Clusters of galaxies are visible tracers of the network of matter in the Universe, marking the high-density regions where filaments of dark matter join together. In the hierarchical scenario of large–scale structure, clusters form via merging of smaller clumps and accretion of material from large scale filaments (e.g., Borgani & Guzzo 2001; Evrard & Gioia 2002). From the observational side, signatures of past merging processes are found in cluster substructure and evidence of ongoing cluster mergers is rapidly accumulating (e.g., Böhringer & Schuecker 2002; Buote 2002; Girardi & Biviano 2002; Evrard 2004).

Over the past few years significant progress has been made to extend the above studies from local to distant clusters. Pioneering analyses suggest that no evidence of dynamical evolution is shown by the cluster population out to $z \sim 0.3$–0.4 (Adami et al. 2000; Girardi & Mezzetti 2001; but cf. Plionis 2002). On the other hand, $z > 0.5$ clusters have more X-ray substructures than lower–z clusters (Jeltema et al. 2005) and most clusters identified at $z \gtrsim 0.8$ show an elongated, clumpy, or possibly filamentary structure (e.g., Donahue et al. 1998; Gioia et al. 1999; Rosati 2004), thus suggesting that present observations are approaching the epoch of cluster formation. Our results on RX J0152.7−1357 at $z \sim 0.8$ add further insights on this issue.

The galaxy cluster RX J0152.7−1357 was discovered in the ROSAT Deep Cluster Survey (RDCS, Rosati et al. 1998) in the ROSAT PSPC field rp60000rn00 observed in January 1992. It was independently discovered in the Wide Angle ROSAT Pointed Survey (WARPS, Ebeling et al. 2000) and reported in the Bright SHARC survey (Romer et al. 2000). It also appeared in the list of X-ray extended sources obtained from *Einstein* IPC data by Oppenheimer et al. (1997).

The BeppoSax observations were used to derive a cluster X-ray bolometric luminosity $L_{X,bol} = (22 \pm 5) \times 10^{44}$ erg s^{-1} ($h = 0.5$ and $q_0 = 0.5$) and a gas temperature $kT = 6.46^{+1.74}_{-1.19}$ keV (Della Ceca et al. 2000). RX J0152.7−1357 is characterized by

⋆ Based in part on observations carried out at the European Southern Observatory using the ESO Very Large Telescope on Cerro Paranal (ESO programs 166.A-0701, 69.A-0683, and 72.A-0759) and the ESO New Technology Telescope on Cerro La Silla (ESO program 61.A-0676).

a complex morphology with at least two cores, both in the optical and X-ray data as recovered by Keck imaging and Beppo-SAX data (Della Ceca et al. 2000). Observations with Chandra also show a complex structure in the intra-cluster medium with the presence in the central cluster region of two peaks in the X-ray emission 95″ apart (North-East: RA = $1^h52^m44^s.18$, Dec = $-13°57'15''.84$; South-West: RA = $1^h52^m39^s.89$, Dec = $-13°58'27''.48$ [J2000.0]), and a possible third peak to the East (RA = $1^h52^m52^s.42$, Dec = $-13°58'5''.52$ [J2000.0]), see Maughan et al. (2003). The existence of an Eastern peak was confirmed by spectroscopic VLT data and an independent analysis of the Chandra data by Demarco et al. (2005), who detect it at the $>3\sigma$ c.l. in X-rays (see their Fig. 1). Chandra observations gave a gas temperature for the North-East and South-West central X-ray clumps of $kT = 5.5^{+0.9}_{-0.8}$ keV and $kT = 5.2^{+1.1}_{-0.9}$ keV, respectively (Maughan et al. 2003). A complex structure with several clumps is also shown by the gravitational lensing analysis of Jee et al. (2005): in particular, the mass clump A corresponds to the Eastern X-ray peak.

There is a lot of evidence to suggest that RX J0152.7−1357 may be undergoing a merger: the displacement between peaks of gas distribution and of galaxy/dark matter distribution (Maughan et al. 2003; Jee et al. 2005); the possible presence of a shock front (Maughan et al. 2003); the presence of galaxies showing a very recent star formation episode (Jørgensen et al. 2005); the segregation of star-forming and non star-forming galaxies probably induced by the intra-cluster medium interaction (Homeier et al. 2005).

Demarco et al. (2005) performed an extensive spectroscopic survey of RX J0152.7−1357 based on observations carried out with FORS1 and FORS2 on the ESO Very Large Telescope, obtaining more than 200 redshifts in the cluster field. Their analysis shows that RX J0152.7−1357 is characterized by a large velocity dispersion, ∼1600 km s^{-1}, and indicates a very complex structure. In particular, the galaxy populations inhabiting the regions around the three main X-ray peaks are characterized by different kinematical behaviour, in agreement with a cluster merging scenario.

On the basis of Demarco et al. data we went on to investigate the internal dynamics of RX J0152.7−1357. The spatial and kinematical analysis of member galaxies is a powerful way to detect and measure the amount of substructure, as well as to identify and analyze possible pre–merging clumps or merger remnants (Girardi & Biviano 2002, and refs. therein). This optical information is complementary to X-ray information, since galaxies and intra–cluster gas react on different time scales during a merger (see, e.g., numerical simulations by Roettiger et al. 1997; Ricker & Sarazin 2001; Schindler 2002).

The paper is organized as follows. We describe member selection and present our results for global properties of RX J0152.7−1357 in Sect. 2. We present our analysis of internal dynamics in Sect. 3, and discuss our results suggesting a tentative picture of the dynamical status of RX J0152.7−1357 in Sect. 4. We summarize our results in Sect. 5.

Unless otherwise stated, we give errors at the 68% confidence level (hereafter c.l.). Throughout the paper, we assume a flat cosmology with $\Omega_m = 0.3$, $\Omega_\Lambda = 0.7$, and $H_0 = 70$ km s^{-1} Mpc^{-1}. For this cosmological model, 1 arcmin corresponds to 458 kpc at the cluster redshift.

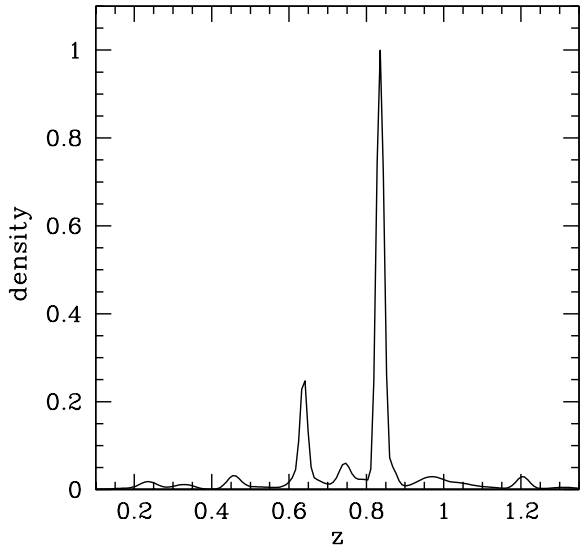

Fig. 1. The redshift galaxy density, as provided by the adaptive-kernel reconstruction method. Unit on the y–axis is normalized to the density of the highest peak.

2. Member selection and global properties

Our data sample consists of the spectroscopic survey of RX J0152.7−1357 presented by Demarco et al. (2005), i.e. 187 galaxies with available redshift (see their Tables 4 and 5). We assumed a typical redshift error of 8×10^{-4} according to the authors' prescriptions.

The identification of cluster members proceeded in two steps, following a procedure already used for nearby and medium–redshift clusters (Fadda et al. 1996; Girardi et al. 1996; Girardi & Mezzetti 2001). First, we performed the cluster–member selection in velocity space by using only redshift information. We applied the adaptive kernel method (Pisani 1993) to find the significant (>99% c.l.) peaks in the velocity distribution. This procedure detects RX J0152.7−1357 as a well-isolated peak at $z = 0.836$ assigning 103 galaxies considered as candidate cluster members (see Fig. 1). Out of non–member galaxies, 61 and 23 are foreground and background galaxies, respectively. In particular, a second significant peak of 31 galaxies is shown at $z = 0.638$ suggesting the presence of a foreground system.

All the galaxies assigned to the RX J0152.7−1357 peak were analyzed in the second step, which uses the combination of position and velocity information. We applied the procedure of the "shifting gapper" by Fadda et al. (1996). This procedure rejects galaxies that are too far in velocity from the main body of galaxies and within a fixed bin that shifts along the distance from the cluster center. The procedure ws iterated until the number of cluster members converged to a stable value. We used a gap of 1000 km s^{-1} – in the cluster rest-frame – and a bin of 0.6 Mpc, or large enough to include 15 galaxies. As for the center, we considered the position of the biweight

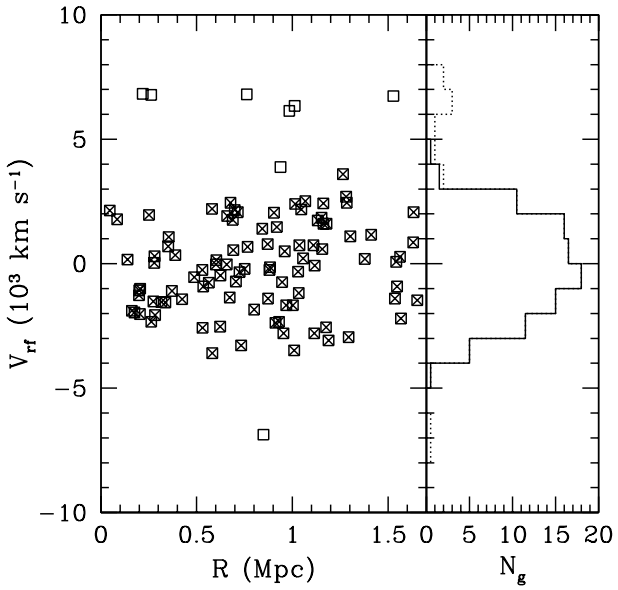

Fig. 2. Galaxies in the main peak of Fig. 1. *Left panel*: rest-frame velocity vs. projected clustercentric distance; the application of the "shifting gapper" method rejects the galaxies indicated by open squares. *Right panel*: velocity distribution of all and member galaxies (dotted and solid histograms, respectively).

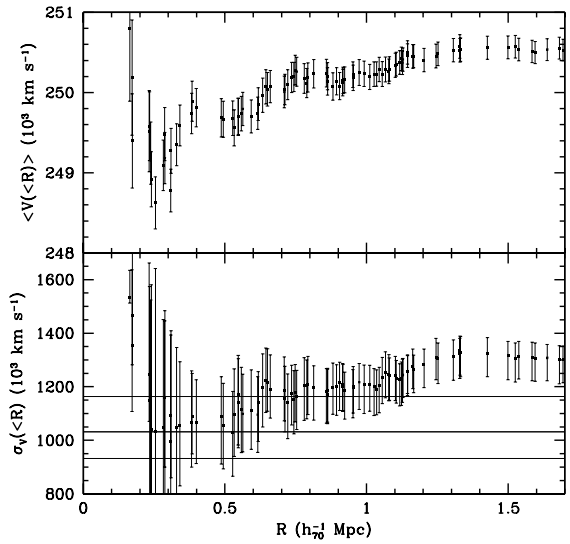

Fig. 3. Integrated mean velocity and LOS velocity-dispersion profiles (*upper and lower panel*, respectively), where $\langle V \rangle$ and σ_V at a given (projected) radius from the cluster center is estimated by considering all galaxies within that radius. The error bands at the 68% c.l. are shown. In the lower panel, the horizontal line represents X-ray temperature with the respective errors transformed into σ_V imposing $\beta_{spec} = 1$ (see Sect. 4).

center, i.e. we performed the biweight mean-estimator (ROSTAT package; Beers et al. 1990) for ascension and declination separately; this center was positioned between the North-East and South-West X-ray peaks (see Sect. 1). The choice of using either one of the two X-ray peaks as cluster center does not affect the final results.

The shifting-gapper procedure rejects eight galaxies to give 95 fiducial members. The list of selected members corresponds to that in Table 4 of Demarco et al. (2005), but excludes galaxies #306, 509, 557, 650, 895, 1146, 1239. Figure 2 shows the plot of rest-frame velocity $V_{rf} = (cz - \langle cz \rangle)/(1 + \langle z \rangle)$ vs. clustercentric distance R of galaxies in the main redshift peak. Finally, we recomputed the biweight center on the 95 cluster members obtaining: RA = $1^h52^m41\overset{s}{.}669$, Dec = $-13°57'58\overset{''}{.}32$ (J2000.0). Unless otherwise stated, we adopted this as cluster center.

By applying the biweight estimator to cluster members (Beers et al. 1990), we computed a mean cluster redshift of $\langle z \rangle = 0.8357 \pm 0.0005$. We estimated the line-of-sight (LOS) velocity dispersion, σ_V, by using the biweight estimator and applying the cosmological correction and the standard correction for velocity errors (Danese et al. 1980). We obtain $\sigma_V = 1322^{+74}_{-68}$ km s^{-1}, where errors were estimated through a bootstrap technique.

To evaluate the robustness of the σ_V estimate, we analyzed the integral velocity dispersion profile (Fig. 3). The value of $\sigma_V(<R)$ sharply varies in the internal cluster region. A similar behaviour is shown by the mean velocity $\langle V(<R) \rangle$ suggesting that a mix of clumps at different redshifts is the likely cause of the high value of the velocity dispersion rather than individual contaminating field-galaxies. A robust value of σ_V was reached in the external cluster regions where the profile flattens, as found for most nearby clusters (e.g., Fadda et al. 1996).

The question of the presence of substructure is deferred to the following sections. Here we assume that the system is in dynamical equilibrium to compute virial global quantities. Following the prescriptions of Girardi & Mezzetti (2001), we assume $R_{vir} = 0.17 \times \sigma_V / H(z) = 2.0$ Mpc for the radius of the quasi-virialized region (see their Eq. (1) after introducing the scaling with $H(z)$, see also Eq. (8) of Carlberg et al. 1997 for R_{200}). Thus the cluster is sampled out to a significant region, i.e. $R_{out} = 0.82 \times R_{vir}$.

We compute the virial mass (Limber & Mathews 1960; see also, e.g., Girardi et al. 1998) using the data for the N_g observed galaxies:

$$M = 3\pi/2 \cdot \sigma_V^2 R_{PV}/G - C, \quad (1)$$

where C is the surface term correction (The & White 1986), and R_{PV}, equal to two times the (projected) harmonic radius, is:

$$R_{PV} = N_g(N_g - 1)/\left(\Sigma_{i \neq j} R_{ij}^{-1}\right), \quad (2)$$

where R_{ij} is the projected distance between two galaxies.

The estimate of σ_V is generally robust when computed within a large cluster region (see Fig. 3 for RX J0152.7−1357 and Fadda et al. 1996 for other examples). The value of R_{PV} depends on the size of the sampled region and possibly on the quality of the spatial sampling (e.g., whether the cluster is uniformly sampled or not). Here we obtain $R_{PV} = (1.45 \pm 0.05)$ Mpc, where the error is obtained via a jacknife procedure. The value of C strongly depends on the radial component of the velocity dispersion at the radius of the sampled region and could be obtained by analyzing the velocity-dispersion profile, although this procedure would require several hundred galaxies. We apply the correction obtained in the

literature by combining data on many clusters sampled out to about $R_{\rm vir}$ ($C/M_{\rm V} \sim 20\%$, Carlberg et al. 1997; Girardi et al. 1998). We obtain $M(<R_{\rm out} = 1.65$ Mpc$) = (2.2 \pm 0.3) \times 10^{15}\ M_{\odot}$. Calling into question the quality of the spatial sampling, one could use an alternative estimate of $R_{\rm PV}$ on the basis of the knowledge of the galaxy distribution. We assume a King-like distribution with parameters typical of nearby/medium–redshift clusters: a core radius $R_{\rm C} = 1/20 \times R_{\rm vir}$ and a slope–parameter $\beta_{\rm fit} = 0.8$, i.e. the volume galaxy density at large radii goes as $r^{-3\beta_{\rm fit}} = r^{-2.4}$ (see G98 and Girardi & Mezzetti 2001). We obtain $R_{\rm PV} = 1.25$ Mpc with a 25% error, thus in agreement with the above direct estimate. The mass is then $M(<R_{\rm out}) = (1.9 \pm 0.5) \times 10^{15} M_{\odot}$, in good agreement with our first estimate.

We can use the second of the above approaches to obtain the mass within the whole assumed virialized region, which is larger than that sampled by observations, $M(<R_{\rm vir} = 2.0$ Mpc$) = (2.2 \pm 0.6) \times 10^{15} M_{\odot}$.

3. Dynamical analysis

3.1. Velocity distribution

We analyze the velocity distribution to look for possible deviations from Gaussianity that could provide important signatures of complex dynamics. For the following tests, the null hypothesis is that the velocity distribution is a single Gaussian. We base our analysis on shape estimators, i.e. the kurtosis and the skewness. As for the kurtosis, we find $K = 2.04 \pm 0.49$, which indicates a $\sim 2\sigma$ departure from a Gaussian distribution (reference value $K = 3$). In addition, we compute the scaled tail index (STI), which also measures the shape of a distribution, but is based on order statistics of the dataset instead of its moments (see, e.g., Beers et al. 1991). This estimator, $STI = 0.860$, indicates that the tails are underpopulated if the parent population is really a single Gaussian with a c.l. between ∼90% and ∼95% (see Table 2 of Bird & Beers 1993). Finally, the W–test (Shapiro & Wilk 1965) also rejects the null hypothesis of a Gaussian parent distribution at the 98% c.l.

Then we investigate the presence of gaps in the distribution, which can be the signature of subclustering. A weighted gap in the space of the ordered velocities is defined as the difference between two contiguous velocities, weighted by the location of these velocities with respect to the middle of the data. We obtain values for these gaps relative to their average size, precisely the midmean of the weighted-gap distribution. We look for normalized gaps larger than 2.25, since in random draws of a Gaussian distribution they arise at most in about 3% of the cases, independent of the sample size (Wainer & Schacht 1978; see also Beers et al. 1991). Three significant gaps (2.312, 2.366, 2.395) in the ordered velocity dataset are detected (see Fig. 4). From low to high velocities the dataset is divided in parts containing 39, 29, 3, and 24 galaxies: thus the gaps individuate three main subsets substantially.

In order to detect the presence of groups within our velocity dataset, we use the Kaye's mixture model (KMM) test (Ashman et al. 1994). The KMM algorithm fits a user-specified number of Gaussian distributions to a dataset and assesses the improvement of that fit over a single Gaussian. In addition, it provides the maximum-likelihood estimate of the unknown n-mode Gaussians and an assignment of objects into groups. KMM is most appropriate in situations where theoretical and/or empirical arguments indicate that a Gaussian model is reasonable. This is valid in the case of cluster velocity distributions, where gravitational interactions drive the system toward a Gaussian distribution. However, one of the major uncertainties of this method is the optimal choice of the number of groups for the partition. Moreover, the algorithm converges only in mixture models with equal covariance matrices for all components, while this is not always true for the heteroscedastic case (see Ashman et al. 1994, for further details).

Our search for significant gaps suggests the presence of two Gaussians (separated by the two very close second and third gaps at $\sim 252 \times 10^3$ km s^{-1}) or possibly three Gaussians (corresponding to the three main subsets). In the homoscedastic case, the KMM algorithm fits a two-group partition by rejecting the single Gaussian at the 97.4% c.l., as obtained from the likelihood ratio test. The three-group partition is fitted at the 97.9% c.l. In the heteroscedastic case, we use the results of the gap analysis to determine the first guess and fit two velocity groups around the guess mean-velocities of 249×10^3 and 254×10^3 km s^{-1}. The algorithm fits a two-group partition at the 99.4% c.l. Similarly, we fit three velocity groups around the guess mean-velocities of 247×10^3, 250×10^3, and 254×10^3 km s^{-1} to obtain a three-group partition at the 97.2% c.l. The high probability value obtained in the heteroscedastic bimodal case suggests the presence of a main cluster of 76 galaxies (KMM1) with the presence of a high-velocity clump of 19 galaxies (KMM2). In turn, the main cluster can be subdivided into two clumps of 19 and 57 galaxies according to the heteroscedastic trimodal case (KMM1a and KMM1b, respectively). Table 1 lists the kinematical properties of these clumps: the three corresponding Gaussians are displayed in Fig. 4. Figure 5 shows that the galaxies of the KMM1a group mainly populate the South–West central region of the cluster. This spatial segregation suggests investigating the velocity field in more detail.

3.2. Velocity field

The cluster velocity field may be influenced by the presence of internal substructures, possible cluster rotation, and the presence of other structures on larger scales, such as nearby clusters, surrounding superclusters, and filaments. Each asymmetry effect could produce a velocity gradient in the cluster velocity field.

To investigate the velocity field of RX J0152.7−1357, we divide galaxies into low- and high-velocity samples by using the median value of galaxy velocities $\bar{V} = 250\,626$ km s^{-1}, and check the difference between the spatial distributions of the two samples. High- and low-velocity galaxies appear segregated in the E–W direction (see Fig. 6). The corresponding spatial distributions are different at the 99.2% c.l. according to the 2D Kolmogorov–Smirnov test (hereafter 2DKS-test; see Fasano & Franceschini 1987, as implemented by Press et al. 1992).

Table 1. Results of Kinematical analysis.

Sample	N_g	$\langle V \rangle$ km s^{-1}	σ_V^a km s^{-1}
Whole system	95	250 530 ± 135	1322^{+74}_{-68}
KMM partitions			
KMM1	76	249 730 ± 124	1080^{+113}_{-53}
KMM2	19	253 634 ± 50	210^{+31}_{-22}
KMM1a	19	247 290 ± 97	408^{+67}_{-50}
KMM1b	57	250 498 ± 102	768^{+97}_{-50}
Dressler – Schectman structures			
DS – SW∗	6	248 338 ± 146	318^{+96}_{-36}
DS – E∗	8	253 488 ± 241	645^{+263}_{-110}
DS – SW	10	248 613 ± 107	317^{+81}_{-47}
DS – E	9	253 429 ± 298	848^{+330}_{-183}
DS – M	76	250 510 ± 149	1293^{+94}_{-69}
Properties of X – ray – centered clumps			
SW – clump(<0.2Mpc)	10	248 535 ± 172	503^{+439}_{-96}
SW – clump(<0.18Mpc)	8	248 713 ± 121	301^{+122}_{-107}
E – clump(<0.4Mpc)	7	253 506 ± 304	710^{+287}_{-117}
NE – clump(<0.4Mpc)	15	251 346 ± 241	888^{+152}_{-75}
Segregation analysis			
passive galaxies	56	250 313 ± 171	1268^{+114}_{-81}
"active"galaxies	39	250 803 ± 226	1410^{+139}_{-125}
SW – clump(passive gals)(<0.3Mpc)	10	248 488 ± 110	321^{+132}_{-59}

[a] We use the biweigth and the gapper estimators by Beers et al. (1990) for samples with $N_g \geq 15$ and with $N_g < 15$ galaxies, respectively (see also Girardi et al. 1993).

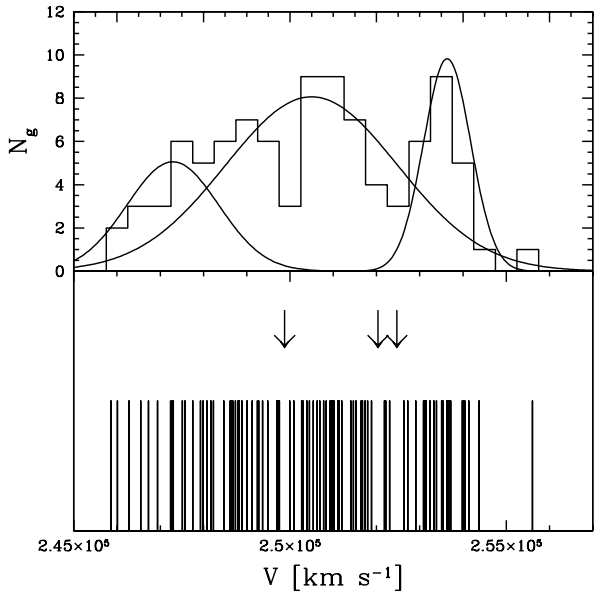

Fig. 4. Velocity distribution of radial velocities for the 95 cluster members. *Bottom panel*: stripe density plot where arrows indicate the position of significant gaps. The first gap lies between 249 757 and 249 997 km s^{-1}, the second between 251 886 and 252 185 km s^{-1}, and the third between 252 305 and 252 635 km s^{-1}. *Top panel*: velocity histogram with a binning of 500 km s^{-1} with the three Gaussians corresponding to KMM1a, KMM1b, and KMM2 in Table 1.

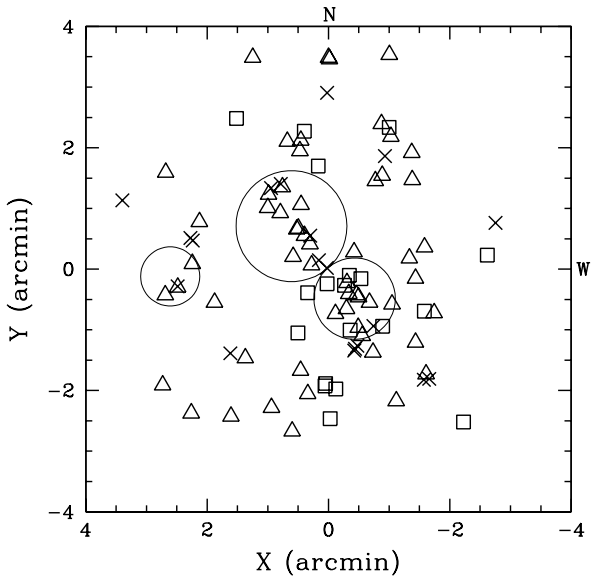

Fig. 5. Spatial distribution on the sky of the 95 member galaxies. Open symbols and crosses indicate galaxies assigned to KMM1 and KMM2 groups, respectively (see text). Squares and triangles indicate KMM1a and KMM1b groups, respectively. The plot is centered on the cluster center defined in Sect. 2. Three circular regions, corresponding to regions of extended X-ray emission, are indicated, too (see Fig. 1 by Demarco et al. 2005).

To estimate the direction of the velocity gradient, we perform a multiple linear regression fit to the observed velocities with respect to the galaxy positions in the plane of the sky (see also den Hartog & Katgert 1996; Girardi et al. 1996). We find a position angle on the celestial sphere of PA = 97° ± 16° (measured counter-clock-wise from North), i.e. higher-velocity galaxies lie in the East-South-East region of the cluster,

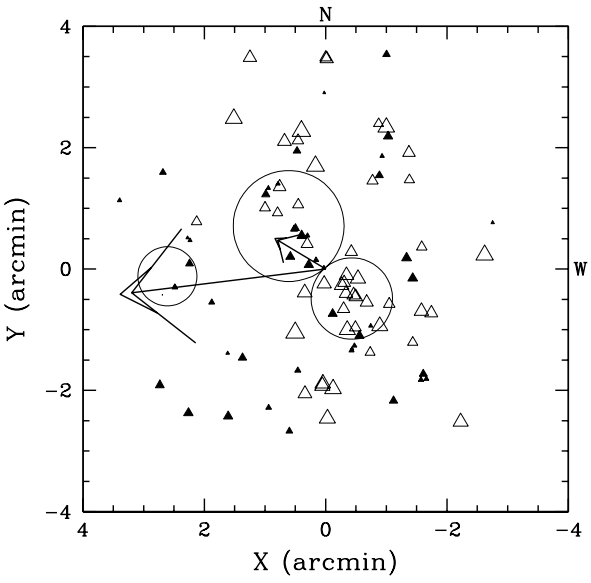

Fig. 6. Spatial distribution on the sky of the 95 member galaxies: the larger the triangle, the smaller the radial velocity. Open and solid triangles indicate galaxies with velocity lower and higher than the median cluster velocity, respectively. The plot is centered on the cluster center. The big and the small arrows indicate the position angle of the cluster gradient as measured over the whole cluster and in internal regions, respectively. The three circles correspond to the regions of extended X-ray emission.

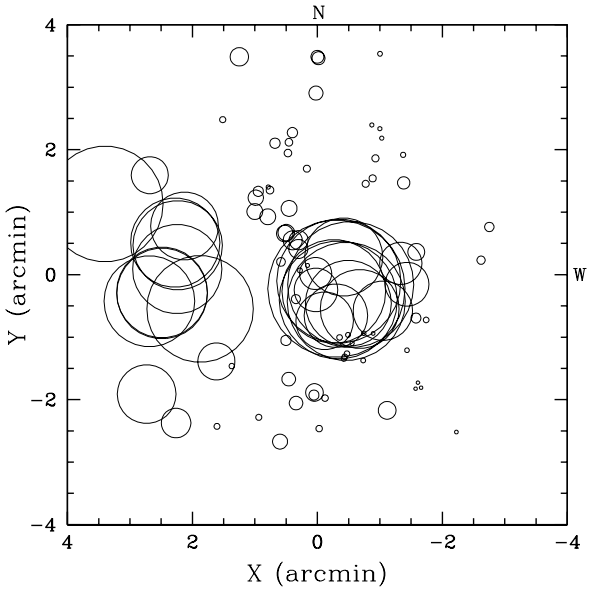

Fig. 7. Spatial distribution of cluster members, each marked by a circle: the larger the circle, the larger is the deviation δ_i of the local parameters from the global cluster parameters, i.e. there is more evidence for substructure (according to the Dressler & Schectman test, see text). The plot is centered on the cluster center.

in agreement with the visual impression of galaxy distribution in Fig. 6. To assess the significance of this velocity gradient, we perform 1000 Monte Carlo simulations by randomly shuffling the galaxy velocities and for each simulation we determine the coefficient of multiple determination (RC^2, see e.g., NAG Fortran Workstation Handbook 1986). We define the significance of the velocity gradient as the fraction of times in which the RC^2 of the simulated data is smaller than the observed RC^2. We find that the velocity gradient is significant at the 98.3% c.l.

We also analyze the central cluster region using 22 galaxies within a radius of 0.4 Mpc. This choice allows us to include the position of both X-ray peaks and to exclude the East region populated by higher-velocity galaxies only. We find a very significant (99.5%) position angle of PA = $59^{\circ}{}^{+28^{\circ}}_{-25^{\circ}}$; i.e. higher-velocity galaxies lie in the direction of the North-East X-ray clump.

3.3. 3D substructure and detection of subclumps

The existence of correlations between positions and velocities of cluster galaxies is a footprint of real substructures. Here we combine velocity and position information to compute the Δ-statistics devised by Dressler & Schectman (1988). This test is sensitive to spatially compact subsystems that have either an average velocity that differs from the cluster mean or a velocity dispersion that differs from the global one, or both. We find $\Delta = 154$ for the value of the parameter which gives the cumulative deviation of the local kinematical parameters (velocity and velocity dispersion) from the global cluster parameters. To compute the significance of substructure, we run 1000 Monte Carlo simulations, randomly shuffling the galaxy velocities, and obtain a value of >99.9%.

This technique also provides information on the positions of substructures. Figure 7 shows the distribution on the sky of all galaxies, each marked by a circle: the larger the circle, the larger the deviation δ_i of the local parameters from the global cluster parameters, i.e. the higher the evidence for substructure. A clump of galaxies with low velocity is the likely cause of large values of δ_i in the region which lies at South–West of the cluster center, i.e. in correspondence of the South–West X-ray peak. The other possible substructure, populated by high-velocity galaxies, lies in the Eastern region.

To assign galaxies to the 3D–subclumps, we resort to the technique developed by Biviano et al. (2002), who use the individual δ_i-values of the Dressler & Schectman method. The critical point is to determine the value of δ_i that optimally separates internal and external substructures. To this aim we consider the δ_i-values of all 1000 Monte Carlo simulations already used to determine the significance of the substructure (see above). The resulting distribution of δ_i is compared to the observed one finding a difference of 99.8% c.l. according to the KS-test. The "simulated" distribution is normalized to produce the observed number of galaxies and compared to the observed distribution in Fig. 8; the latter shows a tail at large values,which is populated by galaxies that presumably are in substructures.

For the selection of galaxies within substructures we chose the value of $\delta* = 3.35$, since only after the rejection of the values $\delta_i > \delta*$ are the observed and simulated distributions no longer distinguishable according to the KS-test. With this choice, 14 galaxies of the cluster are assigned to substructures: six to the central South–West clump (DS-SW*) and eight to the East clump (DS-E*), see Fig. 9. The velocity

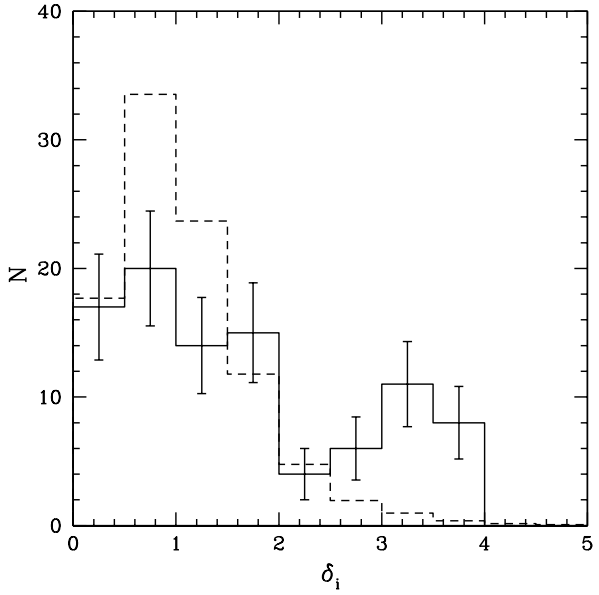

Fig. 8. The distribution of δ_i deviations of the Dressler-Schectman analysis for the 95 member galaxies. The solid line represents the observations, the dashed line the distribution for the galaxies of simulated clusters, normalized to the observed number.

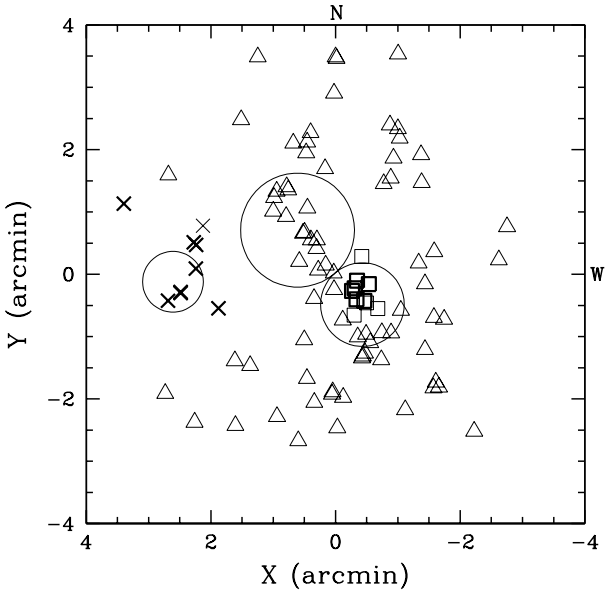

Fig. 9. Spatial distribution on the sky of the 95 member galaxies. Squares and crosses indicate galaxies assigned to the South–West and East clumps detected by the Dressler-Schectman analysis, respectively (DS-SW and DS-E): thick symbols indicate DS-SW* and DS-E*. Triangles indicate the remaining galaxies of the main system (DS-M).

dispersions computed for these structures, $\sigma_V \simeq 300$ km s^{-1} and $\simeq$650 km s^{-1} for DS-S* and DS-E* clumps, respectively, are likely to be considered as lower limits since our analysis does not guarantee the detection of all substructure members.

We also consider a more relaxed criteria, by selecting galaxies with $\delta_i > 3$ as suggested by the histogram of Fig. 8. Table 1 shows that the results for the South–West clump (DS-SW vs. DS-SW*) are very robust, while only one additional galaxy in the Eastern clump (DS-E vs. DS-E*) leads to an increase of 200 km s^{-1} in the velocity dispersion. We also consider the remaining 76 galaxies of the main structure (DS-M). DS-M does not contain significant structure according to the Dressler-Schectman test. However, since we cannot exclude residual contamination from substructure members, its value of velocity dispersion $\sigma_V \sim 1300$ km s^{-1} is likely to be an upper limit.

The Dressler-Schectman results supercede those of the KMM test. Again, there is the presence of a low-velocity clump, and now its South–West position is better defined by detection of the DS-SW clump. The presence of a high-velocity clump is confirmed as located at the East by the detection of the DS-E clump. Moreover, the location of DS clumps coincide well with X-ray peaks of extended emissions.

3.4. Analysis of X-ray – centered clumps

The good spatial agreement between detected galaxy clumps and peaks of X-ray emission prompts us to analyze the profiles of mean velocity and velocity dispersion of galaxy systems corresponding to the South-West, East, and North-East X-ray peaks, i.e. using the position of the X-ray peaks as system-centers (see Figs. 10–12, respectively). This allows an independent analysis of the individual galaxy clumps. An increase

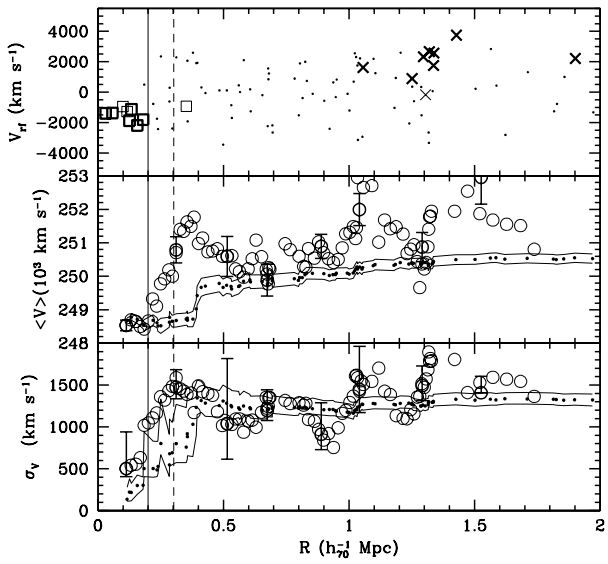

Fig. 10. Kinematical profiles of the SW clump obtained assuming the X-ray peak as center. The vertical line indicates the region likely not contaminated from other clumps (see Sect. 3.4). The dashed vertical line indicates the radius of the extended X-ray emission, as defined by Demarco et al. (2005). *Top panel*: rest-frame velocity vs. projected distance from the clump center: squares and crosses indicate the DS-SW and DS-E as in Fig. 9. Differential (big circles) and integral (small points) mean velocity and LOS velocity-dispersion profiles are shown in *middle and bottom panels*, respectively. For the differential profiles are plotted: a) the values for eight annuli from the center of the clumps, each of 0.2 Mpc (heavy symbols); the current values of each ten galaxies (faint symbols). For the integral profiles, the mean and dispersion at a given (projected) radius from the clump-center is estimated by considering all galaxies within that radius. The error bands at the 68% c.l. are also shown.

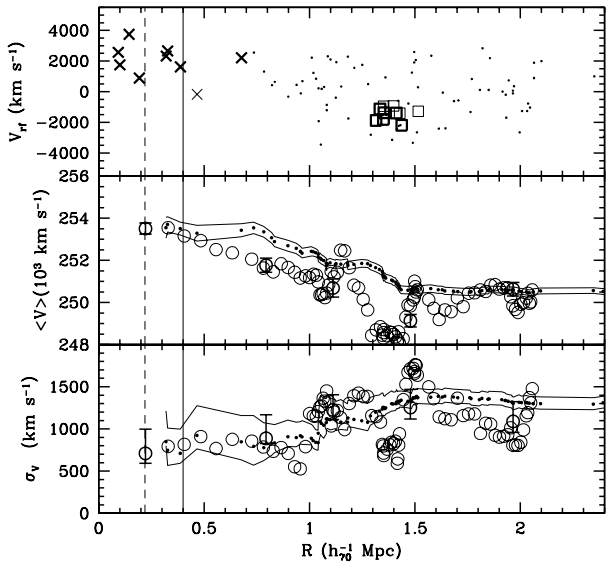

Fig. 11. The same as in Fig. 10, but referring to the E-clump. Note: here the annuli for the differential profiles are 0.45 Mpc each.

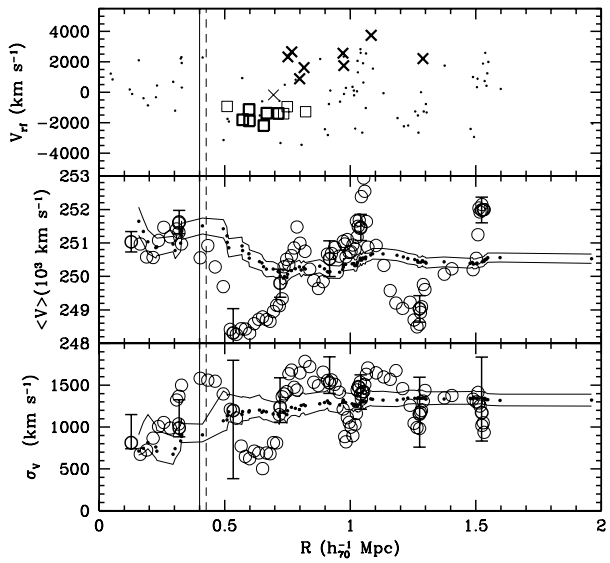

Fig. 12. The same as in Fig. 10, but referring to the central NE-clump.

in the velocity-dispersion profile in their central regions might be due to dynamical friction and galaxy merging (e.g., Menci & Fusco-Femiano 1996; Girardi et al. 1998; Biviano & Katgert 2004) or simply induced by the presence of interlopers or of a secondary clump (e.g., Girardi et al. 1996). The latter hypothesis can be investigated by looking at the behaviour of the mean velocity profile. Figures 10–12 show velocity-dispersion and mean-velocity profiles, as well as regions not likely to be contaminated by other clumps and thus reliable for kinematical analysis. Detailed results of this analysis are included in Table 1 where the clumps are named as SW, E, and NE.

Analysis of the South–West central region indicated the presence of a low-velocity clump with low velocity-dispersion (of 300–400 km s^{-1} according to DS-SW and KMM1a results). Figure 10 shows how the velocity-dispersion increases with the distance from the South-West X-ray peak. The mean velocity shows a sharp change very close to the X-ray peak at ∼0.2 Mpc, suggests a strong contamination of galaxies from other structures. We consider two possible uncontaminated regions: one within 0.2 Mpc, where we find $\sigma_V \simeq 500$ km s^{-1}, and one within 0.18 Mpc, where we find $\sigma_V \simeq 300$ km s^{-1}. Such a sharp change of σ_V is induced just by the rejection of two galaxies, one of which has an anomalously high velocity. The value of σ_V for the SW-clump is further analyzed in Sect. 3.5 and discussed in Sect. 4.1.

Table 2. Virial mass estimates.

Sample	R_{vir}	$M(<R_{vir})$
	Mpc	$10^{14} \times M_\odot$
Whole system	2.0	22 ± 6
SW – clump[a]	0.8	$1.2^{+2.1}_{-0.5}$
SW – clump[b]	0.5	$0.27^{+0.23}_{-0.22}$
E – clump	1.1	$3.5^{+3.0}_{-1.5}$
NE – clump	1.3	$7.0^{+2.9}_{-2.1}$

[a] Using the σ_V computed within 0.2 Mpc(see Table 1). [b] Using the σ_V computed within 0.18 Mpc(see Table 1).

The Dressler-Schectman analysis of the East region indicated the presence of a high-velocity clump with a velocity dispersion of about 600–800 km s^{-1}. By choosing the X-ray peak as center (Fig. 11), the mean velocity changes at ∼0.4−0.5 Mpc from the X-ray peak. Inside this region, we obtain $\sigma_V \sim 700$ km s^{-1} for the E-clump

Figure 12 refers to the region around the North-East X-ray peak. The main mass clump is located at this same position, according to the gravitational lensing analysis (Jee et al. 2005). We have shown that this region is mostly populated by galaxies having velocities intermediate between those of the above clumps, and very likely forms a high velocity dispersion structure (i.e., KMM1b clump in Sect. 3.1, and DS-M system in Sect. 3.3). Figure 12 shows an increase of the integral velocity-dispersion profile at about 0.4 Mpc from the X-ray peak and a corresponding sharp change in the mean velocity. Moreover, galaxies of both DS-SW and DS-E substructures lie beyond 0.4 Mpc from the North–East X-ray peak. Thus, the value $\sigma_V \simeq 900$ km s^{-1}, computed within 0.4 Mpc, should be reliable. The three X-ray clumps differ from each other in mean velocities at a c.l. >99%, according to the means-test (e.g., Press et al. 1992).

Assuming that each of the three galaxy clumps is a system in dynamical equilibrium, for each clump we compute the virial radius and the mass contained inside with the same procedure as was adopted in Sect. 2 (see Table 2). The large uncertainties associated to the mass values are due to poor number statistics.

3.5. Spectral-type segregation

We check for possible spectral-type segregation of galaxies, both in position and in velocity space, by using the classification of Demarco et al. (2005, see their Table 4), i.e. passive galaxies (k), galaxies with significant Balmer lines – most

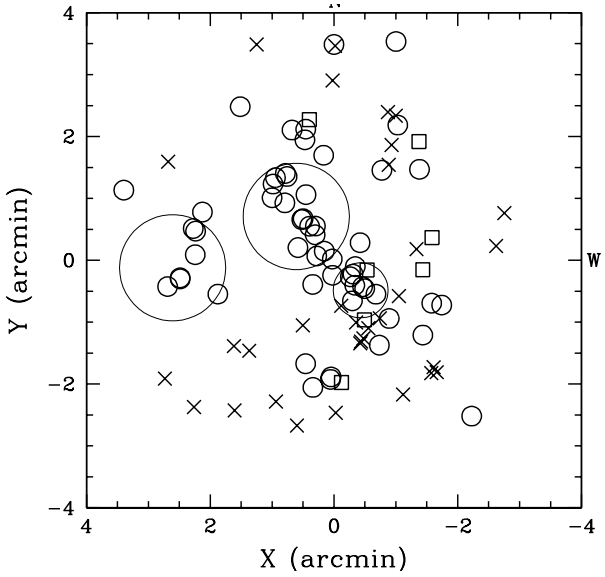

Fig. 13. Projected distribution of the 95 member galaxies. Circles, squares, and crosses indicate passive, post–starburst, and emission–lines galaxies, respectively. The three clumps analyzed in Sect. 3.4 are indicated by the three circles and correspond to the regions likely not to be contaminated by galaxies of other clumps, with radii corresponding to vertical lines in Figs. 10–12.

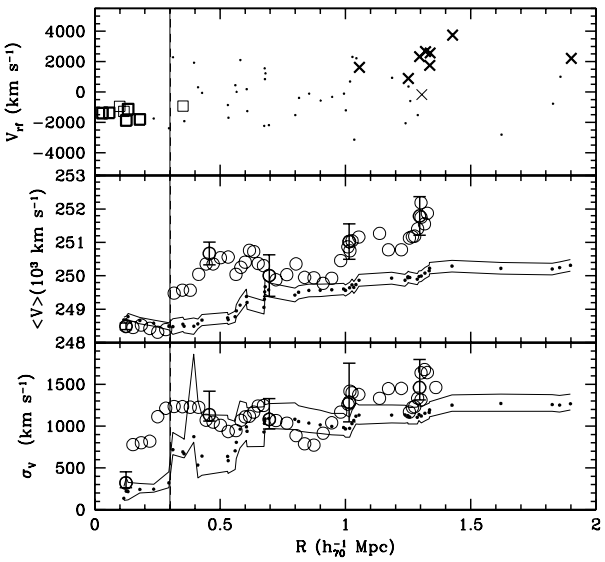

Fig. 14. The same as in Fig. 10, but considering only passive galaxies. Here the annuli for the differential profiles are 0.3 Mpc each.

likely post-starbursts (k+a/a+k) and galaxies with relevant emission lines (e/k+a+[OII]). The sample of cluster members contains 56, 7, and 32 passive, post–starburst, and emission-line galaxies, respectively.

Figure 13 shows the spatial distribution of galaxies of different types. As already noted by Demarco et al., emission-line galaxies avoid the regions of the subclumps (see also Homeier et al. 2005). The same behaviour is shown by post–starburst galaxies. When comparing spatial distributions of passive (k) and "active" (k+a/a+k/e/k+a+[OII]) galaxies, we find a very strong difference: >99.99%, according to the 2DKS-test.

As for the velocity distributions, no difference was found between passive and "active" galaxies, according to the KS-tests. Moreover, mean velocities and velocity dispersions of the two populations (see Table 1) do not significantly differ according to the means- and F-test (e.g., Press et al. 1992). This suggests that our sample of member galaxies is not significantly contaminated by interlopers. In fact, possible field galaxies would preferably contaminate the sample of "active" galaxies, causing a difference in the kinematical properties with respect to the sample of passive galaxies, e.g., enhancing the velocity dispersion or changing the mean velocity.

Finally, we again perform the analysis of mean velocity and velocity-dispersion profiles of Sect. 3.4, by considering only passive galaxies. We draw different conclusions only for the SW-clump. Figure 14 shows that the mean velocity now changes only at ∼0.3 Mpc from the South-West X-ray peak, and the velocity dispersion no longer increases in the central region. Within ∼0.3 Mpc, we compute a value of 321^{+132}_{-59} km s^{-1} for the SW-clump , in good agreement with the lower estimate of σ_V obtained in Sect. 3.4 (see Table 1).

4. Discussion

Out of 187 galaxies with available redshift, we assign 95 members to RX J0152.7−1357. This galaxy selection is more restrictive than the one by Demarco et al. (2005: 102 members giving a velocity dispersion of ∼1600 km s^{-1}) due to our analysis of position and velocity combined together. In particular, we reject a small group of galaxies at $z = 0.864$–0.867. In spite of this more restrictive member selection, the value we obtain for the LOS velocity dispersion is still rather high, $\sigma_V = 1322^{+74}_{-68}$ km s^{-1}, and lies in the high–tail of the σ_V–distribution of nearby/medium redshift clusters (see, e.g., Fadda et al. 1996; Mazure et al. 1996; Girardi & Mezzetti 2001). The position on the $L_{X,bol}$–σ_V plane is consistent with the relation provided by Borgani et al. (1999) for moderately distant clusters and by Wu et al. (1999) for local clusters. As for the σ_V–T_X relation, assuming the density–energy equipartition between gas and galaxies (i.e. $\beta_{spec} = 1$ (e.g., Girardi et al. 1996, 1998; Xue & Wu 2000), where $\beta_{spec} = \sigma_V^2/(kT/\mu m_p)$ with $\mu = 0.58$ the mean molecular weight and m_p the proton mass) our value of σ_V corresponds to $kT = 10.6^{+1.2}_{-1.1}$ keV. This value is more than 2σ higher than the X-ray temperature determined from BeppoSAX observations (Della Ceca et al. 2000) and more than 3σ higher than those of the North-East and South-West X-ray systems as determined from Chandra data (Maughan et al. 2003; Huo et al. 2004). This suggests a strong departure from dynamical equilibrium and, in fact, we find evidence for non–Gaussianity of the velocity distribution, presence of a velocity gradient, and significant substructure.

We find no kinematical difference between passive and "active" galaxy populations, which suggests that our sample of member galaxies is not significantly contaminated by interlopers. In fact, possible field galaxies would preferably contaminate the sample of "active" galaxies, causing a difference in the kinematical properties with respect to the sample of passive galaxies, e.g., enhancing the velocity dispersion or changing the mean velocity.

Instead, our analysis shows that the high value of σ_V is due to the complex structure of this system, i.e. to the presence of three galaxy clumps of different mean-velocity. Using only optical data we detect the low-velocity SW-clump in the central regions and the high-velocity E-clump, which lie close to the South-West and East peaks detected by the X-ray analysis. The North-East X-ray peak is then associated to the main galaxy structure. In particular, the high relative velocity between the NE- and SW-clumps, $V_r = (V_{NE} - V_{SW})/(1+\langle z \rangle) = 1531$ km s^{-1}, explains the high value of σ_V measured in the central cluster region and the presence of a velocity gradient there (see Figs. 3 and 6), while the global velocity gradient is induced by the presence of the high-velocity E-clump in external cluster regions. The presence of the three galaxy clumps was already suggested by Demarco et al. (2005) from inspection of the velocity distribution in relation to the spatial location of galaxies. Moreover, the NE-, SW-, and E-clumps correspond to three clumps in the mass distribution as obtained from the weak lensing analysis (Jee et al. 2005: C, F, and A subclumps, respectively).

As for the mass of the whole cluster, from the global analysis of Sect. 2 we obtain $M(<2.0 \text{ Mpc}) = (2.2 \pm 0.6) \times 10^{15} M_\odot$. Since the system is not virialized, but likely to be bound (see the discussion below). This estimate might overestimate the mass even by a factor two. Adding the mass estimates of each clump within its virial radius (see Table 2, Sect. 3.4), we obtain $M = 1.2^{+0.5}_{-0.3} \times 10^{15} M_\odot$. This estimate should be considered as a lower value within 2.0 Mpc, since it does not consider other small clumps or isolated infalling, bound galaxies, or even the likely possibility that the three clumps extend outside the virial radius. Thus, we conclude that the cluster mass within 2 Mpc lies in the range of $(1.2-2.2) \times 10^{15} M_\odot$, which is typical of very massive clusters (e.g., Girardi et al. 1998; Girardi & Mezzetti 2001).

Our mass estimate is consistent with that of Maughan et al. (2003) of $(1.1 \pm 0.2) \times 10^{15} M_\odot$, based on Chandra X-ray analysis and considering only the two central clumps within 1.4 Mpc. To compare with results from weak lensing analyses, we also compute the projected mass by considering the global cluster geometry as formed by the three clumps at the cluster redshift. Each clump is described by the King–like mass distribution (see Sect. 2) or, alternatively, by a NFW profile where the mass-dependent concentration parameter is taken from Navarro et al. (1997) and rescaled by the factor $1 + z$ (Bullock et al. 2001; Dolag et al. 2004). The mass distribution of each clump is truncated at one virial radius or, alternatively, at two virial radii. In the following we indicate the range of our results. We find the projected mass within 1 Mpc of the center of the main clump (NE-clump) to be $(9-15) \times 10^{14} M_\odot$, higher than that, $5 \times 10^{14} M_\odot$, of Jee et al. (2005), but in agreement with the value $\gtrsim 1 \times 10^{15} M_\odot$ of Huo et al. (2004, see their Fig. 10). Indeed, both Huo et al. and Jee et al. compare their weak lensing results to an isothermal sphere with $\sigma_V = 900$–1000 km s^{-1}, in agreement with the value of σ_V that we measure for the main galaxy clump. However, the weak-lensing mass lies above or below the isothermal sphere mass for Jee et al. and Huo et al., respectively.

4.1. Individual clumps

Our estimate of σ_V for the NE-clump agrees well with that of Demarco et al. (2005) and corresponds to $kT = 4.8^{+1.8}_{-0.4}$ keV, in agreement with the observed gas temperature of ∼6 keV (Maughan et al. 2003; Tozzi et al. 2003; Huo et al. 2004). Similarly, our mass estimate, $M(<R_{vir} = 1.35 \text{ Mpc}) = 7.0^{+2.9}_{-2.1} \times 10^{14} M_\odot$, agrees well with the X-ray mass by Maughan et al. [2003, $M(<1.4 \text{ Mpc}) = 7.0^{+1.7}_{-1.5} \times 10^{14} M_\odot$]. To compare our results with other studies, we rescaled $M(<R_{vir})$ at their radii by using the King–like profile or, alternatively, the NFW profile (see above). In the following, we give the two values obtained from the rescaling, reliable with a 30% lower-error and a 40% upper–error, as derived from the estimate of $M(<R_{vir})$. Our estimates agree well with those of other studies: $M(<0.43 \text{ Mpc}) = (1.9-2.6) \times 10^{14} M_\odot$, cf. with $(2.5 \pm 0.9) \times 10^{14} M_\odot$ by Demarco et al. (2005), based on galaxy dynamics; $M(r < 65'' = 0.496 \text{ Mpc}) = (2.3-2.9) \times 10^{14} M_\odot$, cf. with $(3 \pm 1) \times 10^{14} M_\odot$ by Joy et al. (2001), based on the Sunyaev–Zeldovich effect; $M(r < 0.753 \text{ Mpc}) = (3.8-4.3) \times 10^{14} M_\odot$, cf. with $(2.66 \pm 0.77) \times 10^{14} M_\odot$ by Ettori et al. (2004), based on Chandra X-ray data; $M(r < 1 \text{ Mpc}) = (5.1-5.4) \times 10^{14} M_\odot$, cf. with $\sim 5 \times 10^{14} M_\odot$ by Huo et al. (2004), based on Chandra X-ray data.

As for the SW-clump, the results in the literature are not yet clear. In fact, the X-ray temperature suggests that the NE and the SW clumps are similar in mass (Maughan et al. 2003; Huo et al. 2004), while both the optical analysis by Demarco et al. (2005) and the weak lensing analysis by Jee et al. (2005) find that the SW clump is about half massive than the NE clump. Our analysis of the σ_V–profile gives two alternative values for σ_V: the larger value is consistent with the one found by Demarco et al. (2005, cf. $\sigma_V = 503^{+439}_{-96}$ km s^{-1} vs. their 737 ± 126 km s^{-1}) and with the observed gas temperatures of 5–6 keV (Maughan et al. 2003; Huo et al. 2004), while the lower estimate, $\sigma_V = 301^{+122}_{-107}$, is significantly different. This uncertainty is due to the fact that the σ_V profile increases in central regions (see Fig. 10), and thus the σ_V estimate strongly depends on the considered region. Demarco et al. considered a region (based on X-ray data) larger than our region (based on kinematical data). Our analysis of passive galaxies also gives a small value, $\sigma_V \sim 300$ km s^{-1}, thus suggesting two alternative hypothesis: 1) high values of σ_V are due to galaxy-contamination by other clumps, so that the SW-clump should be considered as a very small group; 2) we are dealing with a very relaxed core hosted in a high-σ_V, massive cluster. The second hypothesis is consistent with observations of nearby clusters where σ_V of the subsample of bright central elliptical galaxies is lower than σ_V of the whole cluster (Biviano & Katgert 2004), a phenomenon possibly due to dynamical friction and galaxy merging (e.g., Menci & Fusco-Femiano 1996). Only a deeper galaxy sample would allow us to better trace and separate the NE and the SW systems and thus discriminate between the two hypotheses. However, the SW-clump appears to be so dense in galaxies that we are inclined to believe in the detection of a cluster-core. In this case, we note that: a) our mass estimate would be an underestimate of the global mass of the Southern cluster; b) our results would be reconciled with high

values of gas temperature and X-ray luminosity (Maughan et al. 2003; Tozzi et al. 2003; Huo et al. 2004).

As for the Eastern clump, the level of X-ray emission in the Chandra image is much lower than those of the NE or the SW clumps (see Fig. 1 of Demarco et al. 2005). In contrast, its gravitational–lensing mass is comparable to that of the South-West clump (see A and F clumps by Jee et al. 2005), and our estimate of velocity dispersion is typical of a massive cluster, $\sigma_V \sim 700$ km s^{-1}. This discrepancy with X-ray luminosity suggests that this galaxy system is far from being virialized, and may be elongated along the LOS (thus giving a high σ_V and a high projected lensing mass), with the gas component not very dense. In particular, the Eastern X-ray peak might be associated to a small group embedded in a large–scale structure filament connecting to the cluster from the ESE region, which is populated by higher velocity – maybe more distant – galaxies (see Fig. 6). In the case of a bound, but non virialized structure, we might have overestimated the mass even by a factor two.

We finally compare the projected mass of the three clumps within a radius of 20′ with the results from weak lensing by Jee et al. (2005). The resulting values for projected masses of the NE-, SW-, and E-clumps lie in the ranges $(1.6-2.3) \times 10^{14}\ M_\odot$, $(0.5-0.7) \times 10^{14}\ M_\odot$, and $(1.0-1.5) \times 10^{14}\ M_\odot$, all values somewhat higher than those reported in Table 2 of Jee et al. for clumps C, F, and A, respectively.

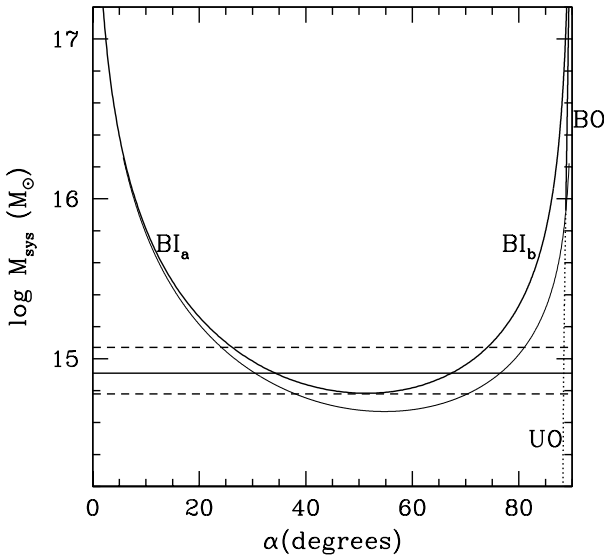

Fig. 15. System mass vs. projection angle for bound and unbound solutions of the two-body model applied to the NE- and SW-clumps (solid and dotted curves, respectively, see text). The thin curve separates the bound and unbound regions according to the Newtonian criterion (above and below the curve, respectively). The horizontal lines give the observational values of the mass system and its 1σ error bands.

4.2. Analytic calculations of the dynamical status

Here, we investigate the relative dynamics of the NE- and SW-clumps in the central cluster region using different analytic approaches which are based on an energy integral formalism in the framework of locally flat spacetime and Newtonian gravity (e.g., Beers et al. 1982). The values of the relevant observable quantities for the two–clump system are: the relative LOS velocity, $V_r = 1531$ km s^{-1}; the projected linear distance between the two clumps, $D = 0.66$ Mpc; the mass of the system obtained by adding the masses of the two clumps each within its virial radius, $M_{sys} = 8.2^{+3.6}_{-2.2} \times 10^{14}\ M_\odot$.

First, we consider the Newtonian criterion for gravitational binding stated in terms of the observables as $V_r^2 D \leq 2GM_{sys} \sin^2\alpha \cos\alpha$, where α is the projection angle between the plane of the sky and the line connecting the centers of two clumps. The faint curve in Fig. 15 separates the bound and unbound regions according to the Newtonian criterion (above and below the curve, respectively). Considering the value of M_{sys}, the NE+SW system is bound between 30° and 77°; the corresponding probability, computed considering the solid angles (i.e., $\int_{30}^{77} \cos\alpha\, d\alpha$), is 47%. We also consider the implemented criterion $V_r^2 D \leq 2GM \sin^2\alpha_V \cos\alpha_D$, which introduces different angles for projection of distance and velocity, not assuming strictly radial motion between the clumps (Hughes et al. 1995). We obtain a binding probability of 44%.

Then, we apply the analytical two-body model introduced by Beers et al. (1982) and Thompson (1982; see also Lubin et al. 1998 for a recent application). This model assumes radial orbits for the clumps with no shear or net rotation of the system. Furthermore, the clumps are assumed to start their evolution at time $t_0 = 0$ with separation $d_0 = 0$, and are moving apart or coming together for the first time in their history; i.e. we are assuming that we are seeing the cluster prior to merging. The bimodal model solution gives the total system mass M_{sys} as a function of α (e.g., Gregory & Thompson 1984). Figure 15 compares the bimodal-model solutions with the observed mass of the system, which is the most uncertain observational parameter. The present bound outgoing solutions (i.e. expanding), BO, are clearly inconsistent with the observed mass. The possible solutions span these cases: the bound and present incoming solution (i.e. collapsing), BI_a and BI_b, and the unbound-outgoing solution, UO. For the incoming case there are two solutions because of the ambiguity in the projection angle α. We compute the probabilities associated to each solution assuming that the region of M_{sys} values between 1σ bands are equally probable for individual solutions: $P_{BIa} \sim 65\%$, $P_{BIb} \sim 35\%$, $P_{UO} < 1 \times 10^{-4}\%$.

There are several limitations to characterizing the dynamics of the central region of RX J0152.7−1357 using these models. For instance, possible underestimates of the masses – e.g., if the clumps extend outside the virial radius or if the SW-clump is only the core of the South-West system (see above) – lead to binding probabilities larger than those computed above. Moreover, the models do not take the mass distribution in the clumps into account when the separation of the clumps is comparable with their size (i.e. at small α) and do not consider the possible effect of the E-clump. Finally, the two-body model breaks down in a regime where the NE- and SW-clumps are already strongly interacting, as suggested by several pieces of evidence: the displacement between peaks of gas distribution and of galaxy/dark matter distribution (Maughan et al. 2003; Huo et al. 2004); Jee et al. 2005); the possible presence of a shock

front (Maughan et al. 2003); the presence of galaxies showing a very recent star formation episode (Jørgensen et al. 2005); the segregation of star-forming and non star-forming galaxies probably induced by the interaction with the intra-cluster medium (Homeier et al. 2005).

Looking only at galaxies, we cannot discriminate between a pre– or post–merging phase since the galaxy component is very robust against mergers; e.g., two clusters can pass through one another without destroying the individual optical components (e.g., White & Fabian 1995; Roettiger et al. 1997). Note, for instance, that the properties of the SW-clump resemble those of cluster-cores destined to survive tidal disruption during the merger: size comparable to the cluster core and mass $\lesssim 0.05\times$ cluster mass (see González-Casado et al. 1994). These cores will be detectable in the host cluster as a substructure for a long time. Since the gas component shows two very distinct entities in the central cluster regions, we presume that the merging is not too advanced, i.e. well before coalescence.

Under the assumption that the two central clumps are already very close, we apply the dynamical models above to the system made of the [(NE+SW)+E] clumps, too. The values of the relevant observable quantities are: $V_r = 1401$ km s^{-1}, $D = 1.09$ Mpc, and $M_{sys} = 11.7^{+4.7}_{-2.6} \times 10^{14}\ M_\odot$. We obtain that the binding probabilities are 48%, and 45%, according to the Newtonian criterion and its implementation, respectively; while the two-body model gives a probability >99.9% for the bound incoming solution.

5. Summary and conclusions

We present the results of the dynamical analysis of the cluster of galaxies RX J0152.7−1357, one of the most massive structures known at $z > 0.8$. The X-ray emission is known to have two clumps in the central regions and a third clump ∼1 Mpc to the East. Our analysis is based on velocities and positions of member galaxies taken from the extensive spectroscopic survey performed by Demarco et al. (2005), i.e. 187 galaxies having redshift in the cluster region.

We find that RX J0152.7−1357 appears as a well–isolated peak in the redshift space at $z = 0.836$ and select 95 cluster members. We compute a value for the LOS velocity dispersion of galaxies, $\sigma_V = 1322^{+74}_{-68}$ km s^{-1}, much larger than expected for a relaxed cluster with an observed X-ray temperature of ∼5−6 keV.

We find evidence that this cluster is far from dynamical equilibrium, as shown by:

- the non Gaussianity of the velocity distribution according to different tests at the 90–98% c.l., as well as the presence of significant velocity gaps;
- the correlation between velocities and positions of galaxies at the >99% c.l., and the presence of a velocity gradient;
- the presence of significant substructures at the >99.9% c.l.

To detect and analyze possible subsystems we used different methods.

- By applying the KMM method, we find that a two-clumps; and most likely a three-clumps partition of the velocity distribution is significantly better than a single Gaussian to describe the velocity distribution. In particular, the galaxies of KMM1a group are mainly located in the SW central region.
- By combining positions and velocities in the Dressler & Schectman statistics, we detect two substructures, corresponding well in location to the SW and E X-ray peaks, in addition to the main cluster component identified with the NE X-ray peak.
- Taking advantage of X-ray peak determination, we analyze the three galaxy clumps centered in these peaks through the profiles of mean velocity and velocity dispersion. This analysis allows us to estimate the clump region that is not likely to be contaminated by galaxies of other clumps and to evaluate the kinematical properties.

In summary, our analysis shows that the high value of σ_V is due to the complex structure of RX J0152.7−1357, i.e. to the presence of three galaxy clumps of different mean-velocity. Using optical data, we detect a low-velocity clump (with $\sigma_V = 300$–500 km s^{-1}) in the central SW region and a high-velocity clump (with $\sigma_V \simeq 700$ km s^{-1}) in the E region, nicely matching the position of the SW and E peaks detected in the X-ray emission. The central NE X-ray peak is associated to the main galaxy structure having intermediate velocity and $\sigma_V \sim 900$ km s^{-1}. The three clumps differ from each other in mean velocities at a c.l. >99% (relative LOS velocities are >1000 km s^{-1}).

The mass of the whole system within 2 Mpc is estimated to be $(1.2$–$2.2) \times 10^{15}\ M_\odot$, where the upper and lower limits come from the virial analysis of the cluster as a whole and from the sum of virial masses of the three individual clumps, respectively.

Analytic calculations, based on the two-body model, indicate that the system is most likely bound, destined to merge. In particular, we suggest that the SW clump is not a small group, but rather the dense core of a massive cluster able to survive tidal disruption during the merger.

In conclusion, RX J0152.7−1357 reveals a very complex structure with several clumps most likely destined to merge in a very massive cluster. Our results lend further support to the picture that massive clusters at $z > 0.8$ are dynamically complex and, therefore, likely to be young. This indicates that we are approaching the epoch at which such massive structures take their shapes from the evolution of the cosmic web. Ongoing extensive spectroscopic surveys of such systems at $z \sim 1$ and beyond, combined with detailed analyses of their gaseus and dark matter components (now possible with weak lensing analysis of HST-ACS data; Jee et al. 2005; Lombardi et al. 2005), will shed new light on cluster formation processes.

Acknowledgements. We thank Andrea Biviano, Massimo Ramella, and Paolo Tozzi for useful discussions. We are grateful to the anonymous referee for helpful comments. This work was been partially supported by the Italian Space Agency (ASI), by the Istituto Nazionale di Astrofisica (INAF) through grant D4/03/IS, and by the Istituto Nazionale di Fisica Nucleare (INFN) through grant PD-51.

References

Adami, C., Holden, B. P., Castander, F. J., et al. 2000, A&A, 362, 825
Ashman, K. A., Bird, C. M., & Zepf, S. E. 1994, AJ, 108, 2348
Beers, T. C., Geller, M. J., & Huchra, J. P. 1982, ApJ, 257, 23
Beers, T. C., Flynn, K., & Gebhardt, K. 1990, AJ, 100, 32
Beers, T. C., Forman, W., Huchra, J. P., Jones, C., & Gebhardt, K. 1991, AJ, 102, 1581
Bird, C. M., & Beers, T. C. 1993, AJ, 105, 1596
Biviano, A., & Katgert 2004, A&A, 424, 779
Biviano, A., Katgert, P., Thomas, T., & Adami, C. 2002, A&A, 387, 8
Böhringer, H., & Schuecker, P. 2002, in Merging Processes in Galaxy Clusters, ed. L. Feretti, I. M. Gioia, & G. Giovannini (The Netherlands: Kluwer Ac. Pub.), Observational Signatures and Statistics of Galaxy Cluster Mergers
Borgani, S., & Guzzo, L. 2001, Nature, 409, 39
Borgani, S., Girardi, M., Carlberg, R. G., Yee, H. K. C., & Ellingson, E. 1999, ApJ, 527, 561
Bullock, J. S., Kolatt, T. S., Sigad, Y., et al. 2001, MNRAS, 321, 559
Buote, D. A. 2002, in Merging Processes in Galaxy Clusters, ed. L. Feretti, I. M. Gioia, & G. Giovannini (The Netherlands: Kluwer Ac. Pub.), X-ray Observations of Cluster Mergers
Carlberg, R. G., Yee, H. K. C., Ellingson, E., et al. 1997, ApJ, 476, L7
Danese, L., De Zotti, C., & di Tullio, G. 1980, A&A, 82, 322
Della Ceca, R., Scaramella, R., Gioia, I. M., et al. 2000, A&A, 353, 498
Demarco, R., Rosati, P., Lidman, C., et al. 2005, A&A, 432, 381
den Hartog, R., & Katgert, P. 1996, MNRAS, 279, 349
Dolag, K., Bartelmann, M., Perrotta, F., et al. 2004, A&A, 416, 853
Donahue, M., Voit, G. M., Gioia, I. M., et al. 1998, ApJ, 502, 550
Dressler, A., & Shectman, S. A. 1988, AJ, 95, 985
Ebeling, H., Voges, W., Böhringer, H., et al. 1996, MNRAS, 281, 799
Ebeling, H., Jones, L. R., Perlman, E., et al. 2000, ApJ, 534, 133
Ettori, S., Tozzi, P., Borgani, S., & Rosati, P. 2004, A&A, 417, 13
Evrard, A. E. 4004, in Clusters of Galaxies, ed. J. S. Mulchaey, A. Dressler, & A. Oemler (UK: Cambridge Univ. Press) Galaxy clusters as probes of cosmology and astrophysics
Evrard, A. E., & Gioia, I. M. 2002, in Merging Processes in Galaxy Clusters, ed. L. Feretti, I. M. Gioia, & G. Giovannini (The Netherlands: Kluwer Ac. Pub.)
Fadda, D., Girardi, M., Giuricin, G., Mardirossian, F., & Mezzetti, M. 1996, ApJ, 473, 670
Fasano, G., & Franceschini, A. 1987, MNRAS, 225, 155
Gioia, I. M., Henry, J. P., Mullis, C. R., Ebeling, H., & Wolter, A. 1999, AJ, 117, 2608
Girardi, M., & Mezzetti, M., 2001, ApJ, 548, 79
Girardi, M., & Biviano, A. 2002, in Merging Processes in Galaxy Clusters, ed. L. Feretti, I. M. Gioia, & G. Giovannini (The Netherlands: Kluwer Ac. Pub.) Optical Observations of Cluster Mergers
Girardi, M., Biviano, A., Giuricin, G., Mardirossian, F., & Mezzetti, M. 1993, ApJ, 404, 38
Girardi, M., Fadda, D., Giuricin, G., et al. 1996, ApJ, 457, 61
Girardi, M., Giuricin, G., Mardirossian, F., et al. 1998, ApJ, 505, 74
Gonzalez-Casado, G., Mamon, G., & Salvador-Solé, E. 1994, ApJ, 433, 61
Gregory, S. A., & Thompson, L. A. 1984, ApJ, 286, 422
Homeier, N. L., Demarco, R., Rosati, P., et al. 2005, ApJ, 621, 651
Hughes, J. P., Birkinshaw, M., & Huchra, J. P. 1995, ApJ, 448, 93
Huo, Z., Xue, S.-J., Xu, H., Squires, G., & Rosati, P. 2004, AJ, 127, 1263
Jee, M. J., White, R. L., Beniítez, N., et al. 2005, ApJ, 618, 46
Jeltema, T. E., Canizares, C. R., Bautz, M. W., & Buote, D. A. 2005, ApJ, 624, 606
Jörgensen, I., Bergmann, M., Davies, R., et al. 2005, AJ, 129, 1249
Joy, M., LaRoque, S., Grego, L., et al. 2001, ApJ, 551, 1
Limber, D. N., & Mathews, W. G. 1960, ApJ, 132, 286
Lombardi, M., Rosati, P., Blakeslee, J. P., et al. 2005, ApJ, 623, 42
Lubin, L. M., Postman, M., & Oke, J. B. 1998, AJ, 116, 643
Maughan, B. J., Jones, L. R., Ebeling, H., et al. 2003, ApJ, 587, 589
Mazure, A., Katgert, P., den Hartog, P., et al. 1996, A&A, 310, 31
Menci, N., & Fusco-Femiano, R. 1996, ApJ, 472, 46
NAG Fortran Workstation Handbook, 1986 (Downers Grove, IL: Numerical Algorithms Group)
Navarro, J. F., Frenk, C. S., & White, S. D. M. 1997, ApJ, 490, 493
Oppenheimer, B. R., Helfand, D. J., & Gaidos E. J. 1997, AJ, 113, 2134
Pisani, A. 1993, MNRAS, 265, 706
Plionis, M. 2002, ApJ, 572, 67
Press, W. H., Teukolsky, S. A., Vetterling, W. T., & Flannery, B. P. 1992, in Numerical Recipes, Second edition (Cambridge University Press)
Ricker, P. M., & Sarazin, C. L. 2001, ApJ, 561, 621
Roettiger, K., Loken, C., & Burns, J. O. 1997, ApJS, 109, 307
Romer, A. K., Nichol, R. C., Holden, B. P., et al. 2000, ApJS, 126, 209
Rosati, P. 2002, in Clusters of Galaxies, ed. J. S. Mulchaey, A. Dressler, & A. Oemler (UK: Cambridge Univ. Press), X-ray clusters at high redshift
Rosati, P., Della Ceca, R., Norman, C., & Giacconi, R. 1998, ApJ, 492, L21
Schindler, S. 2002, in Merging Processes in Galaxy Clusters, ed. L. Feretti, I. M. Gioia, & G. Giovannini (The Netherlands: Kluwer Ac. Pub.), Mergers of Galaxy Clusters in Numerical Simulations
Shapiro, S. S., & Wilk, M. B. 1965, Biometrika, 52, 591
Tozzi, P., Rosati, P., Ettori, S., et al. 2003, ApJ, 593, 705
The, L. S., & White, S. D. M. 1986, AJ, 92, 1248
Thompson, L. A. 1982, in Early Evolution of the Universe and the Present Structure, ed. G. O. Abell, & G. Chincarini (Dordrecht: Reidel), IAU Symp., 104
Wainer, H., & Schacht, S. 1978, Psychometrika, 43, 203
White, D. A., & Fabian, A. C. 1995, MNRAS, 273, 72
Wu, X.-P., Xue, Y.-J., & Fang, L.-Z. 1999, ApJ, 524, 22
Xue, Y.-J., & Wu, X.-P. 2000, ApJ, 538, 65